

A novel algorithm for semi-automatic segmentation of plant leaf disease symptoms using digital image processing

J. G. A. Barbedo¹

Received: 22 January 2016 / Accepted: 24 May 2016
© Sociedade Brasileira de Fitopatologia 2016

Abstract A new computer algorithm is proposed to differentiate signs and symptoms of plant disease from asymptomatic tissues in plant leaves. The simple algorithm manipulates the histograms of the H (from HSV color space) and a (from the L*a*b* color space) color channels. All steps in the algorithmic process are automatic, with the exception of the final step in which the user decides which channel (H or a) provides the better differentiation. An in-depth analysis of the problem of disease symptom differentiation is also presented, in which issues such as lesion delimitation, illumination, leaf venation interference, leaf ruggedness, among others, are thoroughly discussed. The proposed algorithm was tested under a wide variety of conditions, which included 19 plant species, 82 diseases, and images gathered under controlled and uncontrolled environmental conditions. The algorithm proved useful for a wide variety of plant diseases and conditions, although some situations may require alternative solutions.

Keywords Leaf symptoms · Disease diagnosis · Color space transformations · Color histograms

Introduction

Digital image processing techniques are gaining importance in agricultural applications. Significant research effort has been focused on the detection and diagnosis of plant diseases and

Section Editor: Paul D. Esker

✉ J. G. A. Barbedo
jayme.barbedo@embrapa.br

¹ Embrapa Agricultural Informatics, Av. André Tosello, 209 - C.P. 6041, Campinas, SP 13083-886, Brazil

on the measurement of disease severity for more than three decades (Nilsson 1980, 1995; Lindow and Webb 1983; Price and Osborne 1990; Olmstead et al. 2001; Ricker 2004). The advantages and disadvantages of several applications of image analysis specifically for plant disease assessment have been thoroughly reviewed (Bock et al. 2010).

Digital image processing-based methods for disease diagnosis and measurement rely on accurate segmentation of diseased and healthy tissue. The first step in the segmentation of disease symptoms¹ during image analysis is choosing the appropriate color space. In general, conventional color images are stored using the RGB (Red-Green-Blue) color space. This widely used format does not always convey enough information to allow adequate image segmentation. As a result, a transformation to more appropriate color spaces is often applied in order to generate a more suitable representation of the image under consideration. There are many color spaces, and it is possible to create original ones that can improve accuracy of segmentation. However, most methods reported use either the HSV (Hue-Saturation-Value, also known as HSI, where “value” is replaced with the name “intensity”) or the L*a*b* (Lightness and two channels representing opposing color dimensions) color channels. After the transformation, usually only one of the channels is used in segmentation, with H from the HSV color space and a* (or simply a) from the L*a*b* color space being the most commonly employed. Some commercially available systems for measuring plant disease symptoms, such as Assess software (v. 2.0) (Lamari 2002), allow the user to choose the desired channel.

Once the channel has been defined, segmentation can proceed. There are several segmentation methods, including

¹ For simplification, the word *symptom* is used here in a broad sense to encompass not only plant-related symptoms of disease, but also portions of the pathogens and respective structures.

thresholding, clustering, region growth, watershed, and others (Gonzalez and Woods 2007). Due to the characteristics of the problem of segmenting disease symptoms on plant leaves, thresholding, which is considered the simplest of the segmentation methods, is usually preferred. Thresholding, also referred to as binarization, consists of defining one or more threshold value(s) that define the range of pixel values that are associated with the objects of interest, such that only these remain after the thresholding procedure. There are many challenges in determining thresholds, which explains why this value is often defined manually (Bock et al. 2008; Cui et al. 2010; Kwack et al. 2005; Contreras-Medina et al. 2012). The negative impact of the automated thresholding using a relatively rigid thresholding system, such as the one available in Assess (Lamari 2002), was highlighted (Bock et al. 2009). Other authors assume that the characteristics of the images to be processed using a specific method will not change considerably, and thus adopt a fixed threshold (Barbedo 2014; De Coninck et al. 2012). Finally, some approaches attempt to be more flexible by adaptively calculating the threshold according to the characteristics of the images (Camargo and Smith 2009; Huang 2007; Patil and Bodhe 2011; Zhang and Meng 2011), which is the approach used in the algorithm proposed in this study.

The dynamic calculation of the ideal threshold according to the characteristics of the image is not a trivial task, given the variety of conditions that can be experienced in practice. Huang (2007) tackled the problem by applying an exponential transform to the image, with arithmetic manipulation of the resulting color channels to ensure the lesions of interest were isolated. Zhang and Meng (2011) proposed an improved Adaboost algorithm to segment the image into four zones, in order to take into account the variations in color and texture presented by lesions caused by the citrus canker. Some methods explore the histograms generated from the grayscale representation of a suitable color channel to determine the best threshold. Patil and Bodhe (2011) used the so-called triangle method applied to the histogram obtained from channel H of HSI color space to calculate the threshold. The same channel, together with two modified versions of the I_3 channel from the $I_1I_2I_3$ color space (Ohta et al. 1980), were used by Camargo and Smith (2009) to generate a histogram of intensities (Prewitt 1970), whose local maxima, mean and standard deviation values were used to determine the thresholds for each channel.

The method proposed here is based on grayscale histograms, in this case using the H and a channels (from the HSV and $L^*a^*b^*$ color space). A major difference between the proposed approach and its predecessors is that while the latter were either designed to tackle very specific problems or were tested using only one plant species and a small pool of disease symptoms, the algorithm proposed here was intended to deal with a wide variety of conditions, and was tested using

19 plant species and 82 different diseases. Thus, the robustness of the algorithm to a diversity of situations was a primary objective.

The aims of this work were to: 1) develop a novel method for segmenting disease symptoms from healthy tissue; 2) perform image analysis using the new algorithm on a diverse of plant species and diseases to evaluate its accuracy and robustness; and 3) discuss on the potential and limitations of the H and a channels in the context of symptom segmentation on diseased plant leaves.

Material and methods

Image database

The database included images of 82 different diseases or examples of pest damage on 19 plant species (Table 1). All images were captured using a variety of retail digital cameras, with resolutions ranging from 1 to 24 MPixels. The resulting 8-bit images were stored in RGB format.

Of the 938 images, only 11 were used to develop and tune the algorithm, one from each 10 corn diseases, and a single one from citrus' sooty mold. The corn disease images were selected in the beginning of the study when only those images were available. As the database increased, those 10 original images seemed to represent adequately the variety of symptoms in the database, with the exception of sooty mold symptoms which was then included. Prior to segmentation, the leaves of interest were manually selected and isolated from the rest of the image. There are several methods for automatic leaf segmentation (Grand-Brochier et al. 2013). However, automated methods are not consistently accurate and may introduce errors that could impact the algorithm's performance, hence the choice of a manual approach for the step of removing the background.

Description of the proposed algorithm

The algorithm has several stages (Fig. 1). The first step was removal of pixels along the edges of the leaves, which was achieved by applying erosion using a 5-pixel diameter disk as the structuring element. These pixels were removed because, even with manual segmentation of the leaf, the edge zone might present some inconsistencies that could cause issues in image analysis. This procedure may remove some pixels associated with symptoms, but since the number of pixels removed is small, there will be little impact on the accuracy of the final results.

The second step was to transform the RGB image to the HSV and $L^*a^*b^*$ color spaces, from which only channels H and a , respectively, were considered. At this point, the images were no longer in the 8-bit unsigned integer format (pixel

Table 1 Information for an image database of plant diseases and respective number of images of each plant-pathogen interaction used in the development and validation of a semi-automatic method that segments disease symptoms from healthy tissue

Plant species (common name)	Common disease name	Pathogen name (binomial)	Image use	
			Development	Validation
<i>Piper nigrum</i> (Black pepper)	Anthracnose	<i>Colletotrichum spp.</i>	0	1
<i>Phaseolus vulgaris</i> (Common Bean)	Anthracnose	<i>Colletotrichum lindemuthianum</i>	0	21
	Cercospora leaf spot	<i>Cercospora sp.</i>	0	2
	Common bacterial blight	<i>Xanthomonas axonopodis</i> pv. <i>phaseoli</i>	0	25
	Rust	<i>Uromyces appendiculatus</i>	0	2
	—	<i>Hedylepta indicata</i>	0	5
	Target leaf spot	<i>Corynespora cassiicola</i>	0	24
	Bacterial spot	<i>Xanthomonas axonopodis</i> pv. <i>vignicola</i>	0	2
	Web blight	<i>Thanatephorus cucumeris</i>	0	7
	Powdery mildew	<i>Erysiphe polygoni</i>	0	12
	Bean golden mosaic	<i>Begomovirus sp.</i>	0	12
	Phytotoxicity (pesticide)	—	0	8
<i>Anacardium occidentale</i> (Cashew)	Anthracnose	<i>Colletotrichum gloeosporioides</i> Penz. & Sacc	0	7
	Powdery mildew	<i>Erysiphe polygoni</i>	0	5
	Stem bleeding disease	<i>Lasiodiplodia theobromae</i>	0	3
<i>Manihot esculenta</i> (Cassava)	Cassava bacterial blight	<i>Xanthomonas axonopodis</i> pv. <i>manihotis</i>	0	7
	Cercospora leaf spot	<i>Cercospora henningsii</i>	0	7
	Cassava vein mosaic	<i>Cassava vein mosaic virus</i>	0	17
	Powdery mildew	<i>Erysiphe polygoni</i>	0	1
<i>Citrus spp</i> (Citrus)	Alternaria brown spot	<i>Alternaria alternata</i> f. sp. <i>citri</i>	0	2
	Citrus canker	<i>Xanthomonas axonopodis</i> pv. <i>citri</i>	0	9
	Sooty mold	<i>Capnodium spp.</i>	1	1
	Leprosis	<i>Citrus leprosis virus</i> (<i>CiLV</i>)	0	13
	Citrus greasy spot	<i>Mycosphaerella citri</i>	0	3
	Scab	<i>Elsinoë fawcettii</i>	0	2
<i>Cocos nucifera</i> (Coconut)	—	<i>Aceria guerrerensis</i>	0	7
	—	<i>Aspidiotus destructor</i>	0	5
	—	<i>Drechslera incurvata</i>	0	2
	Large verrucose	<i>Coccostromopsis palmicola</i>	0	10
	Cylindrocladium pteridis leaf spot	<i>Cylindrocladium pteridis</i>	0	5
	Whitefly	<i>Aleurodicus destructor</i>	0	3
	Coconut rot	<i>Lasiodiplodia theobromae</i>	0	2
	Phytotoxicity (pesticide)	—	0	2
<i>Coffea arabica</i> (Coffee)	Leaf miner	<i>Leucoptera coffeella</i>	0	12
	Cercospora Leaf Spot	<i>Cercospora coffeicola</i>	0	43
	Rust	<i>Hemileia vastatrix</i>	0	17
	Bacterial blight	<i>Pseudomonas syringae</i> pv. <i>garcae</i>	0	37
	Blister spot	<i>Colletotrichum gloeosporioides</i>	0	8
	Brown leaf spot	<i>Phoma costaricensis</i>	0	25
<i>Zea mays</i> (Corn)	Anthracnose	<i>Colletotrichum graminicola</i>	1	6
	Bushy stunt	<i>Dalbulus maidis</i>	1	2
	Tropical rust	<i>Physopelta zaea</i>	1	13
	Southern corn rust	<i>Puccinia polysora</i>	1	14
	Gibberella ear rot	<i>Gibberella zaea</i>	1	2
	Southern corn leaf blight	<i>Bipolaris maydis</i>	1	44
	Phaeosphaeria Leaf Spot	<i>Phaeosphaeria maydis</i> f. imp. <i>Phyllosticta</i> sp	1	30
	Diplodia leaf streak	<i>Stenocarpella maydis</i>	1	6
	Physoderma brown spot	<i>Physoderma maydis</i>	1	7
	Northern Leaf Blight	<i>Exserohilum turicum</i>	1	45
<i>Gossypium hirsutum</i> (Cotton)	Grey mildew	<i>Ramularia areola</i>	0	36
<i>Vitis vinifera</i> (Grapevines)	Bacterial canker	<i>Xanthomonas campestris</i> pv. <i>viticola</i>	0	13
	Rust	<i>Phakopsora euvitis</i>	0	8
	Isariopsis leaf spot	<i>Mycosphaerella personata</i>	0	1
	Downy mildew	<i>Plasmopara viticola</i>	0	22
	Powdery mildew	<i>Erysiphe necator</i>	0	29
	Grapevine fanleaf virus	<i>Grapevine fanleaf virus</i>	0	2
<i>Brassica oleracea</i> (Kale)	Alternaria leaf spot	<i>Alternaria brassicace</i>	0	4
	Powdery mildew	<i>Erysiphe polygoni</i>	0	3
<i>Cucumis melo</i> (Melon)	Melon mosaic	<i>Melon mosaic virus</i>	0	1
	Powdery mildew	<i>Erysiphe polygoni</i>	0	5
<i>Elaeis guineensis</i> (Palm tree)	Anthracnose	<i>Colletotrichum sp.</i>	0	1
	Black Sooty Mold	<i>Meliola</i> sp.	0	1
<i>Carica papaya</i> (Papaya)	Anthracnose	<i>Colletotrichum gloeosporioides</i>	0	1
<i>Passiflora edulis</i> (Passion fruit)	Anthracnose	<i>Colletotrichum gloeosporioides</i>	0	7
	Cercospora spot	<i>Cercospora sp.</i>	0	4
	Bacterial spot	<i>Xanthomonas axonopodis</i> pv. <i>passiflorae</i>	0	17

Table 1 (continued)

Plant species (common name)	Common disease name	Pathogen name (binomial)	Image use	
			Development	Validation
<i>Oryza sativa</i> (Rice)	Septoria spot	<i>Septoria passiflorae</i>	0	5
	Rice blast	<i>Magnaporthe grisea</i>	0	4
	Leaf scald	<i>Microdochium oryzae</i>	0	2
<i>Glycine max</i> (Soybean)	Bacterial blight	<i>Pseudomonas savastanoi</i> pv. <i>glycinea</i>	0	3
	Cercospora blight	<i>Cercospora kikuchii</i>	0	5
	Rust	<i>Phakopsora pachyrhizie</i>	0	65
	Corynespora leaf spot	<i>Corynespora cassiicola</i>	0	16
	Myrothecium leaf spot	<i>Myrothecium roridum</i> Tode ex. Fr.	0	2
	Powdery mildew	<i>Microsphaera diffusa</i>	0	49
	Ring spot	<i>Leptosphaeria sacchari</i>	0	2
	Red rot	<i>Colletotrichum falcatum</i>	0	20
	Red stripe	<i>Acidovorax avenae</i> subsp. <i>avenae</i>	0	2
<i>Triticum aestivum</i> (Wheat)	Wheat blast	<i>Magnaporthe oryzae</i>	0	10
	Rust	<i>Puccinia triticina</i>	0	21
	Tan spot	<i>Drechslera tritici-repentis</i>	0	2
	Powdery mildew	<i>Blumeria graminis</i> f. sp. <i>tritici</i>	0	19
Total			11	927

values vary discretely from 0 to 255), but in the 16-bit double format (pixel values vary continuously from 0 to 1).

The third step was to remove the 0.1 % brightest pixels in channel H by making them equal to the value of the brightest pixel that did not belong to such a group. This step was needed in order to correct spuriously bright pixels that sometimes appear as a result of the color transformation process. For the remainder of the algorithm, the grayscale representations of both channels H and a were treated alike.

The fourth step was to improve the contrast of the grayscale images by applying the following equation:

$$Q_{i,j} = (P_{i,j} - \min(P)) / (\max(P) - \min(P)), \quad (1)$$

where P and Q are the original and new values of the pixels respectively, and i and j are the indexes of the pixels. The effect of Eq. 1 was to modify the pixel values so they covered the entire range of possible values (0 to 1).

Thus, in channel H the lesions appear darker compared to the healthy tissue, which is the opposite of channel a . Since the operation applied to both channels was the same, the pixel intensities of channel a were inverted, that is, they were made equal to $1-Q_{i,j}$. Additionally, the backgrounds of both images were made equal to 1. The images before and after the contrast enhancement and pixel value adjustments are shown in Fig. 2.

The fifth step was the construction of the intensity histograms from the grayscale representations of both channels. It was determined experimentally that a 100-bin histogram would be the most appropriate (Fig. 3).

The basic idea behind the segmentation was to find the pixel value that best separates healthy and diseased tissue. In this context, the use of the histogram makes sense because the

healthier, greener tissue will generate one or more peaks that in this case are located towards the right end of the histogram

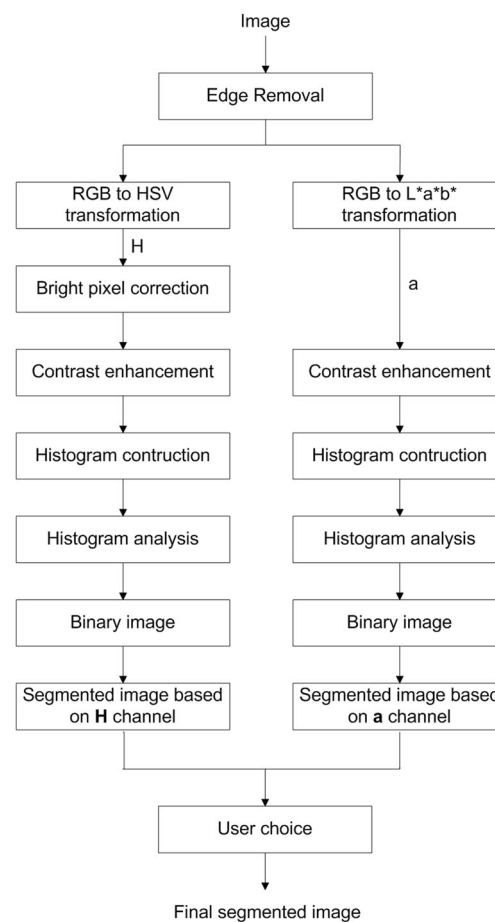


Fig. 1 Process flow of the proposed algorithm for segmenting disease symptoms from healthy tissue of a plant leaf

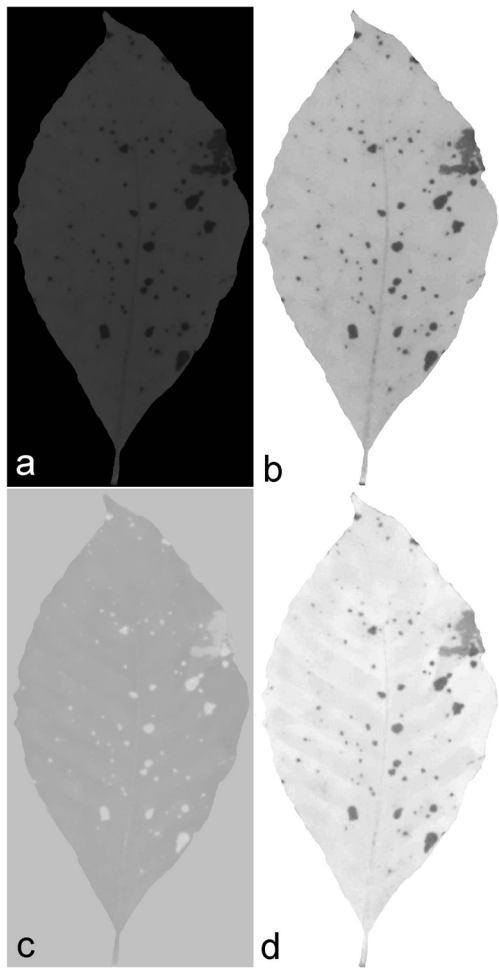
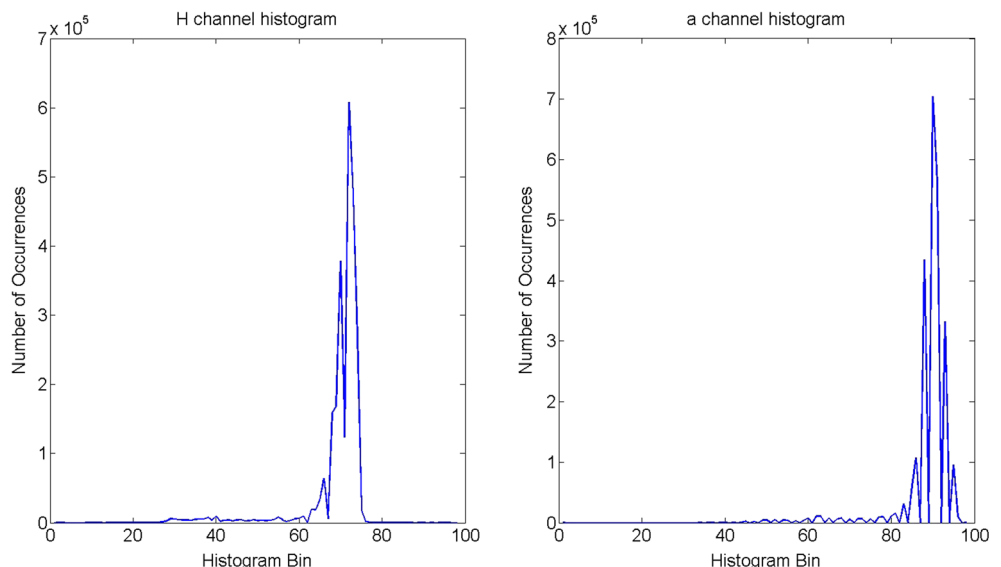


Fig. 2 Illustration of the differences between channels using an image containing symptoms of coffee blaster spot. **a** Original grayscale representation of channel *H*; **b** channel *H* after contrast enhancement and pixel value adjustments; **c** original grayscale representation of channel *a*; **d** channel *a* after contrast enhancement and pixel value adjustments

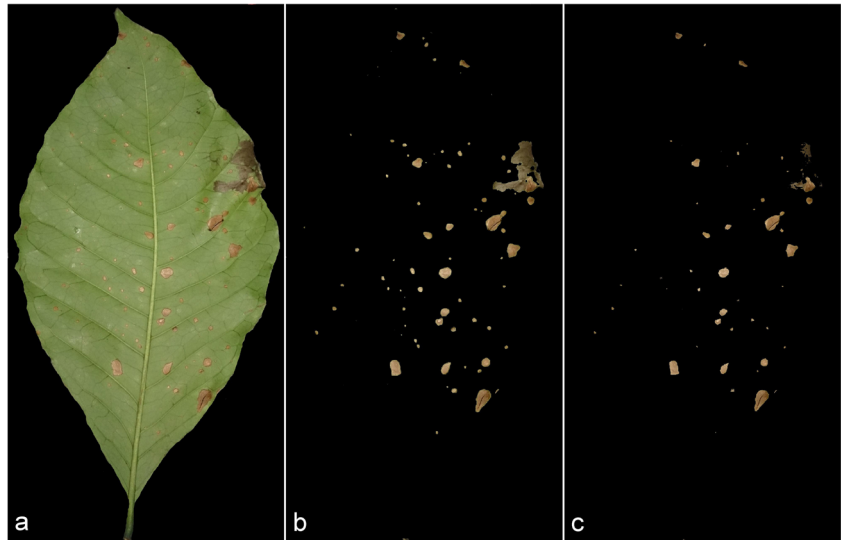
Fig. 3 Intensity histograms showing the distribution differences between the *H* and *a* color channels



(higher value bins). In contrast, diseased tissue tends to generate peaks towards the left end of the histogram (lower value bins). The healthier the leaf as a whole, the more pronounced are the higher peaks. Due to differences in color, shades and illumination, the position of those peaks may vary substantially from sample to sample. With these observations in mind, the following set of rules was created.

A rule was required for the identification of the bin that best represented typical values of green (healthy) pixels in each image, considering that green tissue tends to be represented as a light shade of gray in the grayscale images. The search for such a bin did not follow a perceptual logic, that is, it did not try to identify the shade of green that a human observer would identify as the dominant one for a particular leaf. Instead, it found the bin that would offer the most consistent results given the next steps of the algorithm. Initially, the global maximum was identified, and its location (*B*) and value (*V*) were stored. If $B \leq 40$, the index of the highest bin whose value was larger than $0.2 V$ was taken as reference (*R*). If $B > 40$, *R* was the index of the highest value bin whose value was larger than $0.5 V$. This was necessary because, when the global maximum is located in lower value bins, it indicates that the leaf is severely diseased, that is, there is not much green tissue left, thus generating lower value bins. On the other hand, if the global maximum is located in higher value bins, this indicates that the leaf is still relatively healthy, with green dominating the histogram. Tests revealed that the bin that best separated healthy and diseased tissue was given by $S = 2.R/3$, and the final threshold value was $T = S/100$, since the histogram is composed of 100 bins. An example of segmented images resulting from the application of the thresholds obtained for channels *H* and *a* can be seen in Fig. 4.

Fig. 4 **a** Original image; **b** segmentation of symptomatic from healthy leaf tissue achieved using the channel H ; **c** segmentation achieved using channel a



In the final step of the algorithm, the user chooses which of the two images (that obtained for channel H or a , respectively) provides the most accurate segmentation.

Algorithm validation

The validation of the algorithm was performed using the remaining 927 images. One way to assess the performance of a segmentation algorithm is to manually label the pixels in the image as either healthy or diseased, and then compare the results outputted by the algorithm against those labels (Camargo and Smith 2009). The problem with this approach is that the boundaries of symptoms are not usually well defined. The exact point where the lesion ends and healthy tissue begins becomes a subjective matter. Moreover, in some cases the lesions have zones with different color and texture characteristics, and in some cases only one or a few of those zones are of interest to the user. For example, some lesions have a well defined necrotic area, and an outer ring that gradually fades from yellow to green (Fig. 5).



Fig. 5 Example of a lesion (caused by citrus canker) with distinct regions and fuzzy boundaries

Based on this knowledge, two decisions were taken. First, since the lesion boundaries are subjective, and considering that channels H and a will normally locate different boundaries, it seemed natural that the best approach would be to allow the users to select the boundary that best fits their expectations. Second, in order to take these transition zones into consideration in the tests, the pixels were manually labeled as healthy, diseased or transition. For the pixels classified as transition, any answer provided by the algorithm is considered acceptable. This procedure aimed at a more balanced assessment of the algorithm's performance (Results section).

An issue often encountered during the segmentation process is specular light, which may render parts of the image virtually featureless. The problem is particularly problematic if the leaf has a highly reflective surface. Thus, it is recommended that images be captured in a way that minimizes reflection. Unfortunately, reflection might be unavoidable, and many of the images in the database used were affected. Because specular light artifacts may skew the results, the zones of the images where this effect was more pronounced were manually removed prior to the tests by blackening the bright pixels. Only those specular reflections located exclusively over healthy tissue were removed.

Three experienced plant pathologists, using a computer tool that allowed them to apply thresholds and correct the label of one or several pixels at once, annotated all 938 images. The three annotated versions of each image were combined by a simple majority rule. It is important to note that when the transition zone is extensive, it becomes difficult to determine if that is in fact a transition zone, or it is a sign that the entire leaf is actually dying. This is ultimately a subjective matter, and as such the decision was left to the plant pathologists that labeled the images with the transition zones. The algorithm was evaluated using six tests as follows.

Overall performance

For all 938 images, two statistics, the false negative and false positive rates, were calculated:

$$\text{false negatives (FN)} = (N_m/N) \cdot 100, \quad (2)$$

$$\text{false positives (FP)} = (N_f/N) \cdot 100, \quad (3)$$

where N is the total number of annotated (disease symptom) pixels, N_m is the number of symptom pixels that were not detected by the algorithm, and N_f is the number of pixels that were detected by the algorithm but are not part of the diseased area (according to the expert annotation). It is important to note that no pixel labeled as transition is considered in the calculations, as by definition they cannot generate false positives or negatives.

Image characteristics can vary within the same plant species and disease. As a consequence, FN and FP values also vary from one image to another, thus presenting average values as the main result would have little meaning. Rather than presenting the average FN and FP values, the results are presented in terms of the proportion of images whose FP and FN values fell within one of the following error ranges: low error (LE, 0–5 %), medium-low error (MLE, 5–15 %), medium-high error (MHE, 15–30 %), and high error (HE, 30–100 %). This provides a practical representation of the algorithm's performance and is more readily comprehensible.

It is important to note that, in many cases, the algorithm will succeed with one of the channels, but will fail with the other. Since the user is able to choose the most accurate channel, it does not affect the outcome of the measurement process. The algorithm will only fail when both channels yield unsatisfactory results. The user's choice process itself was not evaluated, as this is ultimately a subjective task that depends on the user's ability and/or needs.

The effect of the transition zone

In order to determine the similarities and differences between the H and a channels regarding the transition zone, the number of pixels classified as “diseased tissue” by channel H (D_H) and channel a (D_a) were determined and combined into a channel ratio (CR):

$$CR = \frac{(D_a - D_H)}{\max(D_a, D_H)}. \quad (4)$$

The closer CR is to zero, the more similar are the results for both channels; the closer CR is to -1 or 1 , the larger the difference between the channels, with negative values indicating that the H channel classified more pixels as diseased, and vice versa.

The effect of specular reflection

As previously mentioned, severe specular reflections were manually removed prior to image analysis. However, in order to quantify the impact of this phenomenon, some tests were performed with the original images. First, pixels corresponding to specular reflection were manually labeled on all images. Then, for each plant species and using each of the color channels, two measurements were made:

$$P_s = \frac{S_p}{S_m}, \quad (5)$$

$$I_s = \frac{S_p}{D_p}, \quad (6)$$

where P_s is the proportion of specular reflection pixels that were classified as diseased by the algorithm, S_p is the number of specular reflection pixels that were classified as diseased by the algorithm, S_m is the number of pixels manually labeled as specular reflection, I_s is the impact of the specular reflection on the segmentation, and D_p is the total number of pixels classified as diseased by the algorithm. P_s quantifies the tendency of the algorithm to detect specular reflections as diseased tissue, and I_s quantifies the impact that specular reflection has on the overall measurement. The closer P_s and I_s are to 1, the more damaging is the specular reflection to the accuracy of the algorithm.

Accuracy and efficiency compared with assess

Two factors were deemed relevant in the comparison with the standard image analysis program Assess, accuracy and speed. Accuracy was measured for both systems using the error ranges described in Section 2.3.1. In the case of the proposed algorithm, the most accurate channel was selected for comparison. Measuring speed was less straightforward, because the time spent to get a result will depend on user skills with computers, familiarity with the systems, characteristics of leaves and symptoms, and other factors. In order to assure consistent results, three individuals with experience in plant disease assessment tested both systems. Before the tests, the subjects were trained and allowed to use the tools until they were fully familiarized with their features. One image for each plant species-disease combination was randomly selected for use in the tests. Finally, the time spent from opening the image to obtaining the final result was measured for each image, and the minimum, maximum and average times spent using each system were computed.

Accuracy compared to other automatic methods

A comparison between the algorithm described here and those proposed by Camargo and Smith (2009); Huang (2007) and

Patil and Bodhe (2011) was performed using the error ranges described in Section 2.3.1.

Agreement and correlation statistics

In order to provide a more synthetic comparison between all methods considered in this work, a linear regression analysis of the type $y = a + bx$ was carried out, where x and y are the percentage of diseased pixels measured by the experienced plant pathologists and by the tested methods, respectively. The statistical analysis, following the one adopted by Bock et al. (2008), included seven measures: Pearson's correlation coefficient (r), which indicates how correlated are the variable being compared; intercept (a from the linear regression equation), whose deviation from 0 indicates a constant systematic error; slope (b from the linear regression equation), whose significant deviation from 1.0 indicates proportional systematic error between assessments (Bock et al. 2008); coefficient of determination (r^2), which indicates the degree to which x explains y ; coefficient of variation (CV), which is a measure for precision; standard error of the estimate (SE), which quantifies random error between assessments; and Lin's concordance correlation (LCC), which quantifies reproducibility.

Results

Using the new algorithm, most disease leaf image measurements had low FP and FN rates. For most diseases, the majority of error rates fell into the LE category. In some cases, the two channels differed in accuracy, as was observed for bean bacterial spot and citrus *alternaria* brown spot. In general, channel H was more accurate when venations were prominent and when the disease caused generalized leaf color changes (Fig. 6), while channel a was more accurate for segmenting very bright and very dark symptoms in low contrast situations.

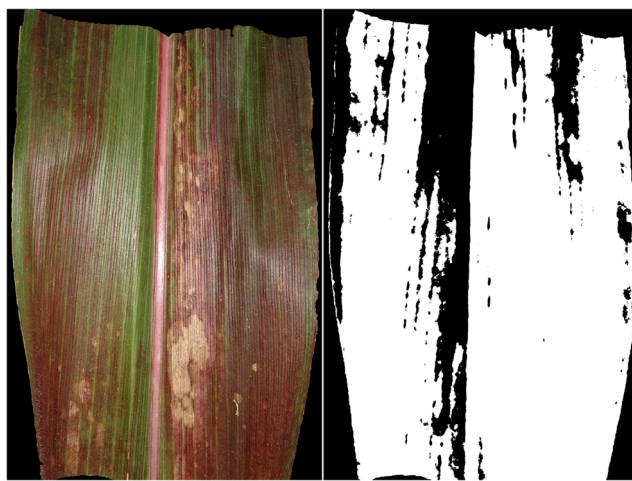


Fig. 6 Example of the segmentation provided by channel H for corn bushy stunt

This observation justifies the use of two channels, as each one can be more accurate under certain conditions. In a few cases, however, both channels failed to accurately segment between healthy and diseased tissue, leading to a high FN rate (false positives were more rare). Two groups of diseases were particularly prone to FN errors: mildews and mosaics. In the case of mildews (mainly powdery mildews), the symptoms (often fungal structures) are small and scattered, being difficult to be detected unless they are heavily clustered. An example of failed detection is shown in Fig. 7. Mosaic diseases, on the other hand, generally lack sufficient contrast to be well detected by the algorithm (Fig. 8).

FNs are much more common compared with FPs, indicating that there is an inherent imbalance in the segmentation process. Specular reflections led to misclassifications of up to 15 % ($I_S=0.15$) of the total number of pixels corresponding to diseased zones when channel a was used, especially in the case of plant species with glossy leaves, including citrus, coconut, coffee, corn, melon, passion fruit and sugarcane (Table 3). Channel H was much less susceptible to specular reflections, with error consistently <1 % of the total number of diseased pixels.

Venations were a source of error, particularly when vein color was closer to yellow or brown rather than green. For some plant species (bean, cashew, coconut, corn, cotton, grapevines, kale, melon, soybean, and sugarcane), venations had a low to moderate impact, affecting fewer than 10 % of the images. In the case of cassava and passion fruit, virtually all images were affected to some degree (Fig. 9). However, in most cases the algorithm, in at least one of the color channels (usually H), is capable of segmenting the symptoms without

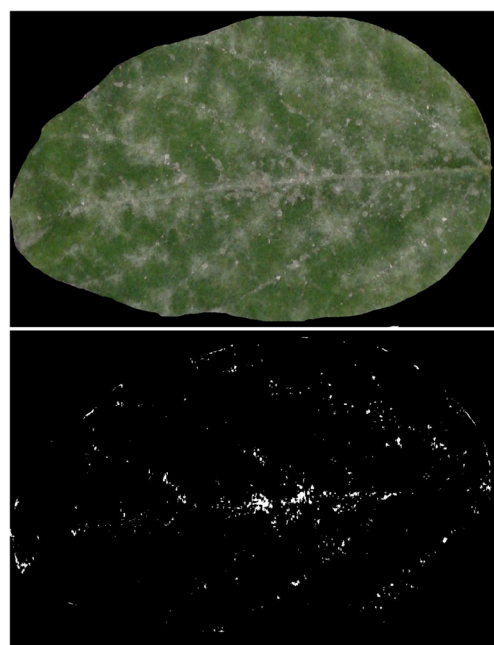


Fig. 7 Example of underdetection caused by powdery mildew

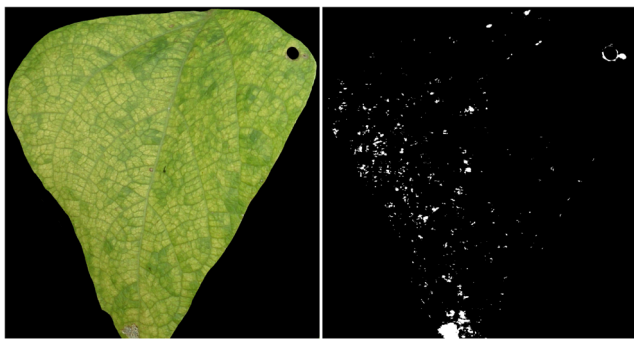


Fig. 8 Example of the segmentation provided by channel *a* for mosaic-like symptoms (bean golden mosaic virus)

taking considerable portions of the veins, which is a major advantage of the two-channel strategy adopted here.

The way pixels in the transition are classified may be important for some applications. One of the main reasons for using two different color channels was due to the fact that each channel takes different portions of the transition zone into consideration, allowing users to choose the option that best fits their needs. In fact, in many cases one of the channels included almost the entire transition zone in the segmentation, while the other one included only the most acute portion of the symptom. Since those differences cannot be visualized in Table 2, as neither case is considered an error, additional tests were conducted in order to better characterize the way the algorithm dealt with the transition zone (Table 4). Channel *a*

tended to consider the transition zone as part of the symptom, while channel *H* tended to consider it healthy tissue. This conclusion is further reinforced by the observation that channel *a* classifies more than 50 % of the transition zone as diseased tissue in 61 % of the images, while channel *H* classifies more than 80 % of the transition zone as healthy tissue in 91 % of the cases (Table 3 and 4).

The manual module of Assess allows the user to control the parameters in order to achieve the best possible answer, which leads to better results compared to the proposed algorithm (Table 5). On the other hand, selecting parameters makes Assess less efficient. The proposed algorithm rarely takes more than 10 s to run, compared with approximately 66 s per image for Assess. Assess offers more accurate results, but it is worth noting that approximately 50 % of the cases for which the algorithm failed, the manual mode of Assess also failed to succeed.

The methods proposed by Camargo and Smith (2009); Huang (2007) and Patil and Bodhe (2011) are automatic and do not include an option for the users to tune parameters or choose the best course of action. Because of that, they tend to be faster, but less accurate compared with the proposed algorithm (Table 6). Camargo and Smith (2009) and Huang (2007) methods had similar average performances, with the former one being more susceptible to false positives, and the latter one being more susceptible to false negatives. The method proposed by Patil and Bodhe (2011) performed slightly worse than the other two.

The results showed above are synthesized in Table 7, which presents a regression analysis for the proposed algorithm, the manual module of Assess, and the three automatic methods. As it can be seen, the statistical analysis confirms the results shown in Tables 5 and 6, that is, the proposed method is more accurate than the automatic ones and less accurate than the manual module of Assess.



Fig. 9 Example of the impact of veins in a passion fruit leaf on segmentation accuracy

Discussion

The 938 images used in this study included a diversity of plant species and diseases, so inevitably some plant-disease combinations were represented by very few images (sometimes only 1). A single or a few images will be unlikely to capture all nuances and variation for a given disease, so the results shown in Table 2 cannot be considered comprehensive. A truly comprehensive database of disease images on different plant species would require substantial effort and coordination. The database we describe here will continue to be expanded and will be made available to the scientific community. Nonetheless, the database was sufficiently large to draw robust conclusions using the new algorithm, which performed accurately with many diseases on a diversity of plant species.

Table 2 Performance of image analysis when using the new algorithm to detect pixels representing diseased symptoms

Plant	Disease name or causal agent	Channel <i>H</i>								Channel <i>a</i>							
		False negatives				False positives				False negatives				False positives			
		LE	MLE	MHE	HE	LE	MLE	MHE	HE	LE	MLE	MHE	HE	LE	MLE	MHE	HE
Black Pepper	Anthracnose	0	100	0	0	100	0	0	0	100	0	0	0	100	0	0	0
Bean	Anthracnose	19	38	24	19	100	0	0	0	43	38	0	19	100	0	0	0
	Cercospora leaf spot	100	0	0	0	100	0	0	0	100	0	0	0	100	0	0	0
	C. bacterial blight	54	42	4	0	100	0	0	0	96	4	0	0	100	0	0	0
	Rust	100	0	0	0	100	0	0	0	100	0	0	0	100	0	0	0
	<i>Hedylepta indicata</i>	40	20	40	0	100	0	0	0	100	0	0	0	100	0	0	0
	Target leaf spot	54	29	17	0	100	0	0	0	100	0	0	0	100	0	0	0
	Bacterial spot	0	50	0	50	100	0	0	0	50	50	0	0	100	0	0	0
	Web blight	100	0	0	0	100	0	0	0	100	0	0	0	100	0	0	0
	Powdery mildew	33	33	26	8	100	0	0	0	33	42	17	8	100	0	0	0
	Golden mosaic virus	25	0	42	33	100	0	0	0	75	0	25	0	67	33	0	0
Cashew Tree	Phytotoxicity	75	25	0	0	100	0	0	0	100	0	0	0	100	0	0	0
	Anthracnose	100	0	0	0	100	0	0	0	100	0	0	0	100	0	0	0
	Powdery mildew	60	0	20	20	100	0	0	0	100	0	0	0	100	0	0	0
	Stem bleeding disease	100	0	0	0	100	0	0	0	100	0	0	0	100	0	0	0
Cassava	Cas. bacterial blight	29	13	29	29	100	0	0	0	44	0	28	28	100	0	0	0
	Cercospora leaf spot	100	0	0	0	0	43	43	14	100	0	0	0	100	0	0	0
	Cas. vein mosaic virus	0	0	0	100	100	0	0	0	0	0	0	100	100	0	0	0
	Powdery mildew	0	100	0	0	0	0	100	0	0	0	0	0	0	100	0	0
Citrus	Alternaria brown spot	50	50	0	0	0	100	0	0	0	0	0	50	50	0	50	0
	Citrus canker	100	0	0	0	67	33	0	0	100	0	0	0	100	0	0	0
	Sooty mold	0	0	0	100	0	0	0	100	100	0	0	0	100	0	0	0
	Leprosis	100	0	0	0	100	0	0	0	100	0	0	0	100	0	0	0
	Citrus greasy spot	33	0	67	0	100	0	0	0	100	0	0	0	100	0	0	0
Coconut	Scab	100	0	0	0	100	0	0	0	50	50	0	0	100	0	0	0
	<i>Aceria guerreronis</i>	100	0	0	0	100	0	0	0	100	0	0	0	100	0	0	0
	<i>Aspidiotus destructor</i>	20	20	20	40	0	0	60	40	60	20	20	20	80	20	0	0
	<i>Dreschslera incurvata</i>	100	0	0	0	50	0	50	0	100	0	0	0	50	0	50	0
	Large verrucose	100	0	0	0	20	30	30	20	100	0	0	0	20	40	30	10
	Cyl. pteridis leaf spot	100	0	0	0	20	60	20	0	100	0	0	0	20	40	40	0
	Whitefly	0	0	0	100	100	0	0	0	100	0	0	0	33	67	0	0
	Coconut rot	0	100	0	0	100	0	0	0	100	0	0	0	100	0	0	0
Coffee	Phytotoxicity	50	0	50	0	100	0	0	0	100	0	0	0	50	50	0	0
	Leaf miner	100	0	0	0	83	17	0	0	100	0	0	0	87	13	0	0
	Cercospora leaf spot	100	0	0	0	65	35	0	0	100	0	0	0	74	26	0	0
	Rust	100	0	0	0	100	0	0	0	100	0	0	0	100	0	0	0
	Bacterial blight	76	19	5	0	100	0	0	0	100	0	0	0	84	16	0	0
Corn	Blister spot	100	0	0	0	100	0	0	0	75	25	0	0	100	0	0	0
	Brown leaf spot	24	72	4	0	100	0	0	0	100	0	0	0	100	0	0	0
	Anthracnose	100	0	0	0	83	17	0	0	100	0	0	0	67	33	0	0
	Bushy stunt	100	0	0	0	0	100	0	0	0	0	0	0	100	100	0	0
	Tropical rust	100	0	0	0	100	0	0	0	85	15	0	0	100	0	0	0
	Southern corn rust	100	0	0	0	79	14	7	0	100	0	0	0	100	0	0	0
Corn	Scab	100	0	0	0	100	0	0	0	100	0	0	0	100	0	0	0
	Southern corn leaf blight	100	0	0	0	68	23	5	4	82	18	0	0	95	5	0	0

Table 2 (continued)

Plant	Disease name or causal agent	Channel <i>H</i>								Channel <i>a</i>								
		False negatives				False positives				False negatives				False positives				
		LE	MLE	MHE	HE	LE	MLE	MHE	HE	LE	MLE	MHE	HE	LE	MLE	MHE	HE	
Cotton	Phaeosphaeria leaf spot	83	17	0	0	93	7	0	0	60	20	20	0	80	20	0	0	
	Diplodia leaf streak	100	0	0	0	80	20	0	0	100	0	0	0	80	20	0	0	
	Physoderma brown spot	42	29	29	0	100	0	0	0	29	57	14	0	100	0	0	0	
	Northern leaf blight	100	0	0	0	64	11	7	18	100	0	0	0	80	9	7	4	
	Grey mildew	42	28	30	0	100	0	0	0	33	28	39	0	100	0	0	0	
	Grapevine	46	38	16	0	92	8	0	0	77	15	8	0	100	0	0	0	
Grapevine	Rust	75	12	0	13	88	12	0	0	75	0	13	12	100	0	0	0	
	Isariopsis leaf spot	100	0	0	0	100	0	0	0	100	0	0	0	100	0	0	0	
	Downy mildew	9	9	14	68	100	0	0	0	36	32	9	23	100	0	0	0	
	Powdery mildew	0	7	24	69	100	0	0	0	3	14	34	49	100	0	0	0	
	Grapevine fanleaf virus	0	100	0	0	100	0	0	0	0	100	0	0	0	100	0	0	0
	Kale	Alternaria brown spot	100	0	0	0	75	25	0	0	100	0	0	0	75	0	25	0
Melon	Powdery mildew	0	0	0	100	100	0	0	0	33	0	33	33	100	0	0	0	
	Melon mosaic	0	0	0	100	100	0	0	0	0	0	0	100	100	0	0	0	
	Powdery mildew	0	0	20	80	100	0	0	0	40	20	20	20	100	0	0	0	
	Palm tree	0	0	100	0	0	0	0	100	100	0	0	0	0	0	0	100	
	Black powdery mildew	0	0	0	100	100	0	0	0	100	0	0	0	100	0	0	0	
	Papaya tree	0	100	0	0	0	0	100	0	0	100	0	0	0	0	100	0	
Passion fruit	Anthracnose	100	0	0	0	71	29	0	0	100	0	0	0	100	0	0	0	
	Cercospora spot	75	25	0	0	100	0	0	0	100	0	0	0	75	25	0	0	
	Bacterial spot	41	59	0	0	100	0	0	0	71	29	0	0	100	0	0	0	
	Septoria spot	40	40	0	20	100	0	0	0	100	0	0	0	100	0	0	0	
	Rice	Rice blast	75	25	0	0	75	25	0	0	75	25	0	0	100	0	0	0
	Leaf scald	50	50	0	0	100	0	0	0	50	50	0	0	50	50	0	0	
Soybean	Bacterial blight	100	0	0	0	100	0	0	0	100	0	0	0	100	0	0	0	
	Cercospora blight	100	0	0	0	100	0	0	0	100	0	0	0	100	0	0	0	
	Rust	51	38	8	3	97	3	0	0	58	37	5	0	95	5	0	0	
	Corynespora leaf spot	100	0	0	0	100	0	0	0	100	0	0	0	100	0	0	0	
	Myrothecium leaf spot	50	50	0	0	100	0	0	0	100	0	0	0	50	50	0	0	
	Powdery mildew	0	2	16	82	100	0	0	0	4	51	10	35	100	0	0	0	
Sugarcane	Ring spot	0	100	0	0	0	50	0	50	50	0	50	0	100	0	0	0	
	Red rot	100	0	0	0	100	0	0	0	100	0	0	0	100	0	0	0	
	Red stripe	100	0	0	0	100	0	0	0	0	50	50	0	100	0	0	0	
	Wheat	Wheat blast	100	0	0	0	80	20	0	0	100	0	0	0	60	20	20	0
	Rust	95	5	0	0	100	0	0	0	86	14	0	0	100	0	0	0	
	Tan spot	100	0	0	0	100	0	0	0	100	0	0	0	100	0	0	0	
	Powdery mildew	47	53	0	0	100	0	0	0	68	32	0	0	100	0	0	0	

Actual pixel status was determined visually by rater consensus. LE, MLE, MHE and MH represent the proportion of images whose false positive and false negative values for the proportion of pixels misidentified fell within the specified category ranges (0–5 %, 5–15 %, 15–30 % and 30–100 %, respectively)

The larger number of false negatives observed in the tests was expected in the context of symptom segmentation, as usually there are more cases where symptoms are almost undetectable, compared with cases where the algorithm is

compelled to measure a greater area than it should (that is, it is inherently less likely to overestimate diseased pixels).

Mildew symptoms are generally small and scattered, causing issues for detection. Ways to deal with the issue caused by

Table 3 Impact of specular reflection on the accuracy of an algorithm for segmenting disease symptoms from healthy tissue

Plant	P_S		I_S	
	Channel H	Channel a	Channel H	Channel a
Black pepper	0	0	0	0
Bean	0	0	0	0
Cashew tree	0.002	0.013	0	0.001
Cassava	0.003	0.019	0	0.002
Citrus	0.090	0.388	0.002	0.022
Coconut tree	0.123	0.455	0.007	0.087
Coffee	0.105	0.444	0.009	0.152
Corn	0.078	0.398	0.006	0.059
Cotton	0	0	0	0
Grapevines	0	0.002	0	0
Kale	0	0	0	0
Melon	0.030	0.155	0.001	0.111
Palm tree	0.088	0.202	0	0.005
Papaya tree	0	0	0	0
Passion fruit	0.099	0.321	0.002	0.085
Rice	0.058	0.225	0	0.013
Soybean	0	0.127	0	0.003
Sugarcane	0.112	0.381	0.005	0.078
Wheat	0.048	0.207	0	0.008

P_S is the proportion of pixels corresponding to specular reflection that were classified as disease symptoms by the algorithm, and I_S is the impact of the specular reflection on the segmentation. Values of P_S and I_S smaller than 0.0005 were considered insignificant and rounded to zero

this symptom type include capturing the leaf's image at close range, either by placing the sensor closer to the leaf or by using optical zooming, so the spores are represented by more pixels. The problem with this approach is that most retail sensors are not well suited for macro photography, so the close-up images often lack the sharpness needed for successful detection using image analysis. Another option is using sensors with higher pixel resolutions. This alternative will only be effective if the optical quality of the sensor is sufficient to generate a sharp image, the drawback being the increased resolution and optical quality will result in higher equipment costs.

Mosaic diseases often produce symptoms that lack contrast with healthy tissue. Considering that channels in 8-bit images will have 256 different levels, it would seem reasonable to detect even small differences. Unfortunately, images from the field contain artifacts produced by variation in illumination, sensor imperfections, debris on the leaf, image compression, etc. Thus, if the algorithm is finely tuned to detect even those small differences, the resulting segmentation will be very noisy. In other words, the contrast between diseased and healthy tissue in the selected color channels has to be high enough so those artifacts have little or no impact on the final result. A possible solution for this problem would be using wavelengths other

than the visible spectrum to differentiate diseased and healthy tissue. The near-infrared band, in particular, has the potential to improve the segmentation process (Peñuelas and Filella 1998; Bauriegel et al. 2011). However, infrared sensors tend to be more expensive than conventional ones.

Specular light is an issue for any digital image processing tool, as it renders parts of the image featureless. The best time to address reflections is during image capture, when avoiding use of a flash may reduce or eliminate the effect. However, in some cases it is impossible to avoid specular reflections. Steddom et al. (2005) showed that despite the negative effect of specular reflections and shadows, removing the affected zones from the image actually decreased the correlation with the disease severity estimated by raters in 8 %. However, in this study specular reflections almost always led to inaccuracy, either by being detected as part of the disease zones, or by causing the histogram-based threshold selection to fail completely (Table 3). Considering the results of Steddom et al. (2005) and our observations, the best course of action would appear to be removal of only the severe specular reflections that are located exclusively over healthy tissue, thus ensuring that the entirety of the diseased zones was subjected to the algorithm, even if obfuscated by glare.

Several plant species that might have issues due to vein color were identified, including bean, cashew, cassava, coconut tree, corn, cotton, grapevines, kale, melon, passion fruit, soybean, and sugarcane. In about 83 % of the cases the algorithm was capable of segmenting the lesions without losing accuracy in at least one of the color channels (usually H), which is a major advantage of the two-channel strategy adopted here. A possible solution for veins is to apply automatic techniques to remove them. A technique was proposed by Barbedo (2014), but was not included in the algorithm because, in some instances, it may be a source of error itself, making it more difficult to analyze the results of the algorithm presented. An alternative would be applying tools such as the Leaf Doctor (Pethybridge and Nelson 2015), which allows the user to manually tune color parameter until the veins are isolated. This option can

Table 4 Distribution of the channel ratio (CR) values, calculated according Eq. 4 and which describe how the algorithm dealt with the transition zone

CR Range	Proportion (%)
-1 to -0.5	3
-0.5 to -0.2	7
-0.2 to 0.2	22
0.2 to 0.5	45
0.5 to 1	23

The second column indicates the proportion of images for which the CR value fell within the interval indicated in the first column

Table 5 Comparison of the performance of the proposed algorithm with the manual segmentation panel of Assess (Lamari 2002) to detect pixels representing diseased symptoms

Plant	Proposed algorithm								Assess							
	False negatives				False positives				False negatives				False positives			
	LE	MLE	MHE	HE	LE	MLE	MHE	HE	LE	MLE	MHE	HE	LE	MLE	MHE	HE
Black pepper	100	0	0	0	100	0	0	0	100	0	0	0	100	0	0	0
Bean	82	12	4	2	97	3	0	0	93	4	3	0	98	2	0	0
Cashew tree	100	0	0	0	100	0	0	0	100	0	0	0	100	0	0	0
Cassava	61	0	18	21	96	4	0	0	83	11	6	0	100	0	0	0
Citrus	88	6	3	3	95	3	0	2	94	6	0	0	100	0	0	0
Coconut tree	95	2	2	1	57	27	15	1	96	4	0	0	92	8	0	0
Coffee	96	4	0	0	91	9	0	0	100	0	0	0	98	2	0	0
Corn	93	5	2	0	77	19	2	2	95	5	0	0	92	7	1	0
Cotton	42	28	30	0	100	0	0	0	66	34	0	0	100	0	0	0
Grapevines	49	27	11	13	100	0	0	0	70	25	5	0	97	3	0	0
Kale	72	0	14	14	86	0	14	0	80	10	10	0	90	5	5	0
Melon	33	17	17	33	100	0	0	0	50	25	13	12	100	0	0	0
Palm tree	100	0	0	0	50	0	0	50	100	0	0	0	100	0	0	0
Papaya tree	100	0	0	0	0	100	0	0	100	0	0	0	100	0	0	0
Passion fruit	93	7	0	0	94	6	0	0	100	0	0	0	94	6	0	0
Rice	67	33	0	0	83	17	0	0	83	17	0	0	100	0	0	0
Soybean	77	15	3	5	91	9	0	0	90	8	2	0	100	0	0	0
Sugarcane	50	25	25	0	100	0	0	0	75	25	0	0	100	0	0	0
Wheat	89	11	0	0	90	5	5	0	93	7	0	0	100	0	0	0

Actual pixel status was determined visually by rater consensus. LE, MLE, MHE and MH represent the proportion of images whose false positive and false negative values for the proportion of pixels misidentified fell within the specified category ranges (0–5 %, 5–15 %, 15–30 % and 30–100 %, respectively)

provide very accurate results, however it demands some time and effort from the user in order to be effective.

Other less common factors may interfere with the algorithm's accuracy. Sharp differences in illumination over the surface of the leaf may cause error. Differences usually result either from the leaf not being flat, so some parts of its surface may receive direct light while others may be partially shadowed, or from other objects casting shadows on the leaf. Washed out images resulting from excessive exposure are also a problem, as many of the distinguishing features of leaf and symptoms may be lost. Depending on the angle of illumination, trichomes may appear very bright and prominently in the image, often being mistaken as symptoms themselves. Extreme image compressions (above 50:1) may result in artifacts whose impact on the algorithm is unpredictable - a more complete discussion on effects of compression can be found in Barbedo (2014).

Computer-aided segmentation can be classified into manual, semi-automatic and automatic. Manual segmentation is operationally defined as when the user has to tune one or several parameter to achieve the desired result. An example of a tool like this is the manual module of the

image processing software Assess (Lamari 2002). The proposed algorithm, on the other hand, is a semi-automatic tool in which the only task performed by the user is choosing which of two outputs provides the best result. This means it is much faster than the manual module of Assess (Table 6). On the other hand, Assess allows the user to control the parameters in order to achieve the most accurate measurement (Table 5). These conclusions are in agreement with those of Martin and Rybicki (1998) and Bock et al. (2009). Furthermore, the automatic module of Assess can result in considerable inaccuracy (Bock et al. 2009). This indicates that the proposed algorithm is more appropriate in situations of high throughput that require speed and for which low to moderate error rates may be acceptable, while systems like the manual module of Assess should be used in applications for which accuracy is paramount.

Despite the superior accuracy of the manual module of Assess, it was not always possible to achieve accurate segmentation. This is usually due to a lack of a color transformation capable of generating an image for which the symptoms can be fully separated from healthy tissue.

Table 6 Comparison of the performance of the new algorithm and the methods proposed by Camargo and Smith (2009); Huang (2007) and Patil and Bodhe (2011) to detect pixels representing symptoms in a variety of plant species

Plant	False Negatives				False Positives				False Negatives				False Positives			
	LE	MLE	MHE	HE												
Proposed Algorithm																
Black pepper	100	0	0	0	100	0	0	0	100	0	0	0	100	0	0	0
Bean	82	12	4	2	97	3	0	0	71	18	7	4	67	20	9	4
Cashew tree	100	0	0	0	100	0	0	0	91	9	0	0	98	2	0	0
Cassava	61	0	18	21	96	4	0	0	48	18	18	16	80	12	8	0
Citrus	88	6	3	3	95	3	0	2	79	5	8	8	95	2	1	2
Coconut tree	95	2	2	1	57	27	15	1	77	17	3	3	60	19	14	7
Coffee	96	4	0	0	91	9	0	0	88	10	1	1	90	10	0	0
Corn	93	5	2	0	77	19	2	2	68	17	12	3	70	15	7	8
Cotton	42	28	30	0	100	0	0	0	30	23	31	16	91	6	3	0
Grapevines	49	27	11	13	100	0	0	0	40	15	25	20	93	6	1	0
Kale	72	0	14	14	86	0	14	0	44	28	14	14	72	14	14	0
Melon	33	17	17	33	100	0	0	0	17	33	17	33	83	17	0	0
Palm tree	100	0	0	0	50	0	0	50	100	0	0	0	50	0	50	0
Papaya tree	100	0	0	0	0	100	0	0	100	0	0	0	0	100	0	0
Passion fruit	93	7	0	0	94	6	0	0	83	10	7	0	91	7	2	0
Rice	67	33	0	0	83	17	0	0	50	33	17	0	83	0	17	0
Soybean	77	15	3	5	91	9	0	0	49	25	10	16	88	10	2	0
Sugarcane	50	25	25	0	100	0	0	0	46	24	20	10	92	8	0	0
Wheat	89	11	0	0	90	5	5	0	77	19	10	4	90	5	5	0
Huang																
Black pepper	100	0	0	0	100	0	0	0	100	0	0	0	100	0	0	0
Bean	60	24	12	4	78	21	9	2	52	28	13	7	61	17	5	5
Cashew tree	93	7	0	0	91	7	2	0	92	8	0	0	90	8	2	0
Cassava	61	0	13	26	66	21	11	12	37	12	39	12	67	17	6	10
Citrus	85	7	8	0	84	6	6	4	77	11	12	0	81	10	5	4
Coconut tree	90	4	6	0	48	18	18	16	73	13	13	1	35	20	13	32
Coffee	93	5	2	0	81	10	9	0	85	12	10	3	85	14	11	0
Corn	74	13	13	0	60	21	13	6	74	8	12	6	33	40	14	13
Cotton	42	20	10	28	90	5	5	0	33	22	22	23	87	11	2	0
Grapevines	45	29	11	15	90	5	3	2	41	18	25	16	93	7	0	0
Kale	72	0	14	14	58	14	14	14	58	14	28	0	58	14	28	0
Melon	33	33	17	17	83	17	0	0	33	17	17	33	83	17	0	0
Palm tree	100	0	0	0	50	0	0	50	50	50	0	0	50	0	50	0
Papaya tree	100	0	0	0	0	100	0	0	0	100	0	0	0	0	100	0
Passion fruit	87	13	0	0	90	7	3	0	85	10	5	0	83	7	7	3
Rice	67	33	0	0	67	33	0	0	67	33	0	0	67	33	0	0
Soybean	76	18	2	4	80	11	5	4	69	11	13	7	75	9	7	9
Sugarcane	46	34	16	4	88	8	4	0	42	30	16	12	84	12	0	4
Wheat	81	15	4	0	79	11	7	3	80	10	0	10	80	13	7	0

Actual pixel status was determined visually by rater consensus. LE, MLE, MHE and MH represent the proportion of images whose false positive and false negative values for the proportion of pixels misidentified fell within the specified category ranges (0–5 %, 5–15 %, 15–30 % and 30–100 %, respectively)

This is most acute when a single threshold is applied to the entire image, but it may happen even if a more

Table 7 Correlation and linear regression coefficients, dispersion statistics (CV and SE) and Lin's concordance correlation coefficient (LCC) for testing agreement between estimates of percent leaf area classified by several methods and estimates by experienced raters

Method	r	Intercept	Slope	r ²	CV	SE	LCC
Proposed	0.95	-1.34	0.87	0.90	42.3	6.62	0.86
Assess (manual)	0.97	-1.14	0.94	0.94	23.1	4.86	0.92
Camargo and Smith	0.90	2.22	0.80	0.81	74.5	7.77	0.82
Huang	0.89	-3.00	0.80	0.79	71.2	7.54	0.82
Patil and Bodhe	0.81	-3.94	0.71	0.66	90.8	10.92	0.70

flexible threshold scheme is adopted. Thus, many of the errors experienced by the proposed algorithm may be unavoidable, no matter the kind of tool that is applied to the segmentation.

The methods proposed by Camargo and Smith (2009); Huang (2007) and Patil and Bodhe (2011) are automatic. Automatic methods will tend to be faster than the new algorithm, although for some images, depending on how fast the user chooses the output, the time differences might be very small. As expected, because the proposed algorithm relies on two color channels from which the most accurate is chosen, the results achieved were superior, particularly in cases where symptoms were either very scattered or very faint.

As noted above, if accuracy is paramount, manual methods like Assess are the best option, but if accuracy and speed are both important, the proposed algorithm is a good alternative. Hybrid solutions may be practical in some situations: for example, if none of the results by the proposed algorithm are satisfactory, a third option may be offered which sends the image directly to a manual tool, where the user manually segments the image for a more accurate measurement.

In conclusion, the semi-automatic method described using the novel algorithm allows flexibility without compromising speed. The algorithm is robust to variations in leaf color, symptom color, illumination differences, etc. Most errors were the result of limitations inherent in the color channels, and some sources of error could not be avoided even if using a fully manual approach. The database of images depicting different diseases on different plant species used in this study will be added to, making it possible to dynamically adapt and improve the algorithm, resulting in a more comprehensive and accurate method. An implementation of the algorithm will be made available in the near future in the web address <<https://www.agropediabrasilis.cnptia.embrapa.br/web/digipathos>>, after the inclusion of a more friendly user interface.

Acknowledgments This work was supported by Embrapa, under grant n. 02.14.09.001.00.00, and also by Fapesp, under grant n. 2013/06884-8.

References

- Barbedo JGA (2014) An automatic method to detect and measure leaf disease symptoms using digital image processing. *Plant Dis* 98: 1709–1716
- Bauriegel E, Giebel A, Geyer M, Schmidt U, Herppich WB (2011) Early detection of *Fusarium* infection in wheat using hyper-spectral imaging. *Comput Electron Agric* 75:304–312
- Bock CH, Parker PE, Cook AZ, Gottwald TR (2008) Visual rating and the use of image analysis for assessing different symptoms of citrus canker on grapefruit leaves. *Plant Dis* 92:530–541
- Bock CH, Parker PE, Cook AZ, Gottwald TR (2009) Automated image analysis of the severity of foliar citrus canker symptoms. *Plant Dis* 93:660–665
- Bock CH, Poole G, Parker PE, Gottwald TR (2010) Plant disease severity estimated visually, by digital photography and image analysis, and by hyperspectral imaging. *Crit Rev Plant Sci* 29:59–107
- Camargo A, Smith J (2009) An image-processing based algorithm to automatically identify plant disease visual symptoms. *Biosyst Eng* 102:9–21
- Contreras-Medina LM, Osornio-Rios RA, Torres-Pacheco I, Romero-Troncoso RJ, Guevara-González RG, Millan-Almaraz JR (2012) Smart sensor for real-time quantification of common symptoms present in unhealthy plants. *Sensors* 12:784–805
- Cui D, Zhang Q, Li M, Hartman GL, Zhao Y (2010) Image processing methods for quantitatively detecting soybean rust from multispectral images. *Biosyst Eng* 107:186–193
- De Coninck BMA, Amand O, Delauré SL, Lucas S, Hias N, Weyens G, Mathys J, De Bruyne E, Cammue BPA (2012) The use of digital image analysis and real-time PCR fine-tunes bioassays for quantification of Cercospora leaf spot disease in sugar beet breeding. *Plant Pathol* 61:76–84
- Gonzalez RC, Woods RE (2007) Digital image processing, 3rd edn. Prentice Hall
- Grand-Brochier M, Vacavant A, Cerutti G, Bianchi K, Tougne L (2013) Comparative study of segmentation methods for tree leaves extraction. In: International Workshop on Video and Image Ground Truth in Computer Vision Applications, Proceedings... New York, 7 p
- Huang KY (2007) Application of artificial neural network for detecting *Phalaenopsis* seedling diseases using color and texture features. *Comput Electron Agric* 57:3–11
- Kwack MS, Kim EN, Lee H, Kim JW, Chun SC, Kim KD (2005) Digital image analysis to measure lesion area of cucumber anthracnose by *Colletotrichum orbiculare*. *J Gen Plant Pathol* 71:418–421
- Lamari L (2002) ASSESS: image analysis software for plant disease quantification, 1st edn. APS Press, St. Paul
- Lindow SE, Webb RR (1983) Quantification of foliar plant disease symptoms by microcomputer-digitized video image analysis. *Phytopathology* 73:520–524
- Martin DP, Rybicki EP (1998) Microcomputer-based quantification of maize streak virus symptoms in *Zea mays*. *Phytopathology* 88:422–427
- Nilsson HE (1980) Remote sensing and image processing for disease assessment. *Prot Ecol* 2:271–274
- Nilsson HE (1995) Remote sensing and image analysis in plant pathology. *Annu Rev Phytopathol* 15:489–527
- Ohta Y, Kanade T, Sakai T (1980) Color information for region segmentation. *Comput Graphics Image Process* 13:222–241
- Olmstead JW, Lang GA, Grove GG (2001) Assessment of severity of powdery mildew infection of sweet cherry leaves by digital image analysis. *HortSci* 36:107–111
- Patil SB, Bodhe SK (2011) Leaf disease severity measurement using image processing. *Int J Eng Technol* 3:297–301
- Peñuelas J, Filella I (1998) Visible and near-infrared reflectance techniques for diagnosing plant physiological status. *Trends Plant Sci* 3:151–156
- Pethybridge SJ, Nelson SC (2015) Leaf doctor: a New portable application for quantifying plant disease severity. *Plant Dis* 99:1310–1316
- Prewitt J (1970) Object enhancement and extraction. In: Lipkin B, Rosenfeld A (eds) Picture processing and psychopictorics. Academic, New York, pp 75–149
- Price TV, Osborne CF (1990) Computer imaging and its application to some problems in agriculture and plant science. *Crit Rev Plant Sci* 9: 235–266
- Ricker MD (2004) Pixels, bits, and GUIs: the fundamentals of digital imagery and their application by plant pathologists. *Plant Dis* 88: 228–241
- Steddom K, Jones D, Rudd J, Rush C (2005) Analysis of field plot images with segmentation analysis: effect of glare and shadows. *Phytopathology* 95:S99
- Zhang M, Meng Q (2011) Automatic citrus canker detection from leaf images captured in field. *Pattern Recogn Lett* 32:2036–2046